Journal Pre-proof

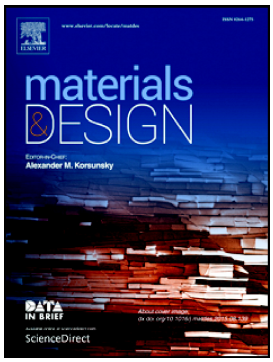

Characterization of elastic, thermo-responsive, self-healable supramolecular hydrogel made of self-assembly peptides and guar gum

Raffaele Pugliese, Fabrizio Gelain

PII: S0264-1275(19)30808-1

DOI: https://doi.org/10.1016/j.matdes.2019.108370

Reference: JMADE 108370

To appear in: *Materials & Design*

Received date: 10 October 2019

Revised date: 15 November 2019

Accepted date: 15 November 2019

Please cite this article as: R. Pugliese and F. Gelain, Characterization of elastic, thermo-responsive, self-healable supramolecular hydrogel made of self-assembly peptides and guar gum, *Materials & Design*(2019), https://doi.org/10.1016/j.matdes.2019.108370

Characterization of Elastic, Thermo-Responsive, Self-Healable Supramolecular Hydrogel made of Self-Assembly Peptides and Guar Gum

Raffaele Pugliese[a], *Fabrizio Gelain*[a,b,*]

[a]*Tissue Engineering Unit, Institute for Stem Cell Biology, Regenerative Medicine and Innovative Therapies-ISBReMIT, Fondazione IRCCS Casa Sollievo della Sofferenza, San Giovanni Rotondo (FG), Italy*

[b]*Center for Nanomedicine and Tissue Engineering (CNTE), ASST Grande Ospedale Metropolitano Niguarda, Milan, Italy*

Corresponding Author

* f.gelain@css-mendel.it

HIGHLIGHTS

- A synthetic biomimetic self-assembling peptide was reinforced through its integration with a naturally occurring polysaccharide guar gum.
- Composite hydrogel showed preserved nanostructured morphology and cross-β structure aggregation typical of SAPs.
- Composite hydrogel showed improved mechanical properties (peaking at 1:1 weight ratio with G'~60 kPa) with self-healing propensity.
- Composite hydrogel exhibited reversible gel-sol transitions in response to thermal stimuli.
- Stretchability of composite hydrogel was extended well beyond 5% strain-limit, typical of standard SAPs.

ABSTRACT

Self-assembling peptides (SAPs) show great promise in regenerative medicine and beyond. Yet, their low mechanical rigidity and limited processability hinder many of their potential applications. In this work we describe the reinforcement of a synthetic biomimetic and β-sheet rich FAQRVPP-LDLK12 SAP by its integration with a naturally occurring polysaccharide - guar gum - to produce a shapeable and thermo-responsive composite hydrogel. Extensive characterization was performed via rheological measurements, CD spectroscopy, FT-IR spectroscopy, and AFM analyses. Composite hydrogels show preserved nanostructured morphology and cross-β structure aggregation typical of SAPs, improved mechanical properties (peaking at 1:1 weight ratio with G'~60 kPa) with self-healing and stress-relaxation propensities: they also exhibit reversible repeatable gel-sol transitions in response to thermal stimuli. Thanks to the dynamic properties of guar gum, stretchability was extended far beyond 5% strain of standard SAPs and processability allowed for the production of knotted threads and long (> 10 cm) flexible sheets. Composite hydrogels of guar gum and SAPs may be added to the growing library of biomimetic SAP hydrogels used in 3D-printing, wound healing, suturing and beyond.

KEYWORDS: self-assembling peptides, guar gum, supramolecular hydrogels, self-healing, thermal responsive, nanofibers.

INTRODUCTION

Hydrogels (natural or synthetic) have historically led the application of biomaterials in medicine and material science.[1] Among them, hydrogels designed using supramolecular principles have a wide impact in various areas, such as tissue engineering,[2] drug delivery,[3] waste-water treatment,[4] and bioelectronics.[5] Supramolecular chemistry - defined by Lehn as "chemistry beyond the molecule" [6] - is based on the rational design of specific and reversible non-covalent molecular recognitions involving hydrogen bonds, hydrophobic interactions, π-π stacking, and van der Waals interactions that can be leveraged to create supramolecular nanomaterials whose physical and chemical properties correlate with those of their building blocks,[7] but that can also make new unexpected ones. In the field of supramolecular biomaterials, scientists have widely used self-assembling peptide (SAPs) hydrogels to demonstrate the broad utility of nanomaterials in biomedical applications.[8] Commonly, SAPs form ordered nano-assemblies in water at concentrations of 1-5% (w/v) yielding to interwoven nanofibers capable of forming hydrogels upon exposure to external shifts in pH, temperature, or salts.[9] SAPs provide a number of advantages, including a relatively ease of synthesis, functionalization with biological moieties typical of native extra-cellular matrix (ECM), an optimal biocompatibility, and bonafide non-immunogenic properties.[10] In particular, SAPs containing alternating hydrophilic and hydrophobic amino acid residues (e.g. RADA16, or KLD12) have enabled pioneering works across a number of different applications.[11-19] Other key examples include peptide amphiphiles (PAs)[20-24] comprising hydrophobic alkyl tails and hydrophilic heads (e.g. palmitoyl-$V_3A_3E_3$-NH_2),[25] multidomain peptides (MDPs) (e.g. $K_2(SL)_6K_2$),[26-29] and peptide-based small-molecule gelators (e.g. Fmoc-FF) making use of non-peptidic structural moieties (namely 9-fluorenylmethoxycarbonyl chloride - Fmoc) to self-

assemble into antiparallel β-sheets amyloid-like fibrils.[30-33] Although these rationally designed supramolecular nanomaterials offer unquestionable advantages as hemostat solutions,[34, 35] nanocarriers of drugs,[36, 37] bone fillers,[38] wound healers,[39, 40] and as injectable scaffolds for the regeneration of injured heart,[41] cartilage[14] and nucleus pulpous,[42] they still face some limitations, like poor mechanical compliance, stiffness and elasticity.[9] We recently introduced chemical cross-linking of SAPs as a new strategy leading to high-performance SAPs, named cross-SAPs, processable into self-standing scaffolds.[43, 44] Thanks to the improved biomechanics of cross-SAPs, our laboratories managed, for the first time, to electrospin cross-linked SAPs into resilient microchannels entirely made of SAPs with tunable functionalization, flexibility and bioabsorption times to suit the specific needs of different applications.[44] Nonetheless, low elastic profiles of bulk materials and long lasting reaction times of some synthetic and natural cross-linkers are being still valid concerns. Aiming to fill this gap we focused our attention on Guar Gum (GG). GG is extracted from the seeds of Cyamopsis Tetragonalobus, belonging to the leguminosae family. It consists of a linear backbone of 1,4-linked β-D-mannopyranosyl units decorated with side-chains of 1,6-linked α-d-galactopyranosyl units-rich in hydroxyl groups.[45] GG features high molecular weight (from 1 MDa to 2 MDa), favorable water solubility, and hydroxyl group-rich side chains, potentially in increasing the intra-molecular cross-links and the overall network entanglement degree.[46] GG solutions are prone to enzymatic and microbial degradation; indeed they have been successfully used as colon-specific delivery systems for dexamethasone,[47] metronidazole,[48] mebendazole,[49] and other anti-inflammatory agents (e.g. indomethacin, doxorubicin hydrochloride).[46, 50] Herein, we tested the effect of GG on the structural and physicochemical properties of a biomimetic β-sheet rich SAP used for nervous regenerative applications,

FAQRVPP-LDLK12.[51] Indeed, FAQRVPP motif derived from Ph.D.-7 phage library, provided functionalized microenvironments with specific biological cues capable of stimulating adult neural stem cell (NSC) adhesion and differentiation,[51] and favored nervous regeneration when injected into rats with acute spinal cord injuries (SCI) without altering the physiological inflammatory response following the initial insult.[51] Hence, aiming to combine the advantages of both SAPs and GG, we obtained and elastic, self-healable, and multi-stimuli responsive hydrogel with mechanical properties superior to both GG and SAP alone. The secondary structures, biomechanics, and morphologies of GG-SAP composite hydrogels were extensively characterized at different weight ratios (e.g. 1:0, 1:0.25, 1:0.5, 1:0.75, 1:1, 1:2, and 1:3) by Fourier transform infrared (FT-IR), circular dichroism (CD), oscillatory stress rheology, and atomic force microscopy (AFM). In particular one mixture (1:1 w/w) can boost the attractive features of GG without compromising the self-assembly propensity of FAQRVPP-LDLK12, leading to intriguing reversible thermo-responsive behavior and high processability into a variety of flexible shapes This study may facilitate the development of polysaccharide-peptide self-assembly with controlled and tunable properties and broaden the number of applications of SAP-based hydrogels.

MATERIALS AND METHODS

General: All reagents and solvents used for the peptide synthesis and characterizations were purchased from commercial sources and used without further purification.

Peptide Synthesis and Purification: The peptide NH_2-FAQRVPPGGGLDLKLDLKLDLK-$CONH_2$ was synthesized by conventional Fmoc solid-phase synthesis (Liberty-Discovery - CEM), using a Rink amide 4-methyl-benzhydrylamine resin (0.5 mmol g^{-1} substitution). Fmoc-

protected amino acids were used at 0.2 M in DMF. Removal of side-chain protecting groups and cleavage were obtained by using a 95:2.5:2.5 mixture of TFA:TIS:H_2O. Raw peptide was subsequently purified to more than 95%, as verified by binary HPLC (Waters) followed by mass spectrometry confirmation (Waters LC-MS Alliance-3100).

Preparation of Guar Gum-Peptide Composite Hydrogels: The peptide and guar gum in the required ratio (final concentration of 1 % w/v) were dissolved in distilled water (GIBCO®), vortexed for 3 min and sonicated for 30 min. For the assembly, 10 % of sodium tetraborate decahydrate ($Na_2B_4O_7 \cdot 10H_2O$, borax, pH 8.5) was added to guar gum-peptide solution slowly. Then the guar gum-peptide solution mixed with borax buffer was left at room temperature until a homogeneously stable borax-guar gum-peptide hydrogel was formed (~15 min). Different composite hydrogels were prepared at diverse guar gum-peptide ratios (e.g. 1:0, 1:0.25, 1:0.5, 1:0.75, 1:1, 1:2, and 1:3).

Rheological Test: Rheological properties of guar gum-peptide hydrogels were carried out using AR-2000ex Rheometer (TA instruments) equipped with a truncated cone-plate geometry (acrylic truncated diameter, 20 mm; angle, 1°; truncation gap, 34 μm). Viscosity of guar gum-peptide samples was measured using a flow step program, at increasing shear rate, to evaluate non-Newtonian behavior of the hydrogels. To evaluate the storage (*G'*) and loss (*G"*) moduli of assembled guar gum-peptide hydrogels, frequency sweep experiments were recorded as a function of angular frequency (0.1-1,000 Hz) at fixed strain of 1 %. The recovery property of guar gum-peptide hydrogels in response to applied shear forces was performed at constant angular frequency (ω=1 Hz) as the following procedure: 10 % (300 s) → 100 % (300 s) → 10 % (300 s) → 100 % (300 s) → 10 % (300 s). To avoid the evaporation of water, mineral oil coated the edge of the cone-plate geometry. Further, the stress-relaxation performance of guar gum-

peptide hydrogels was performed at 5 %, 10 % and 100 % strain held constant and with a deformation rate of 1 mm min^{-1}. The load was recorded as a function of time. Lastly, thermo responsive properties of guar gum-peptide hydrogels were evaluated by heating (25 °C → 80 °C) and cooling (80 °C → 25 °C) cycles as a function of *G'* (T_{rate} = 2 °C min^{-1}, 1% strain, ω =1 Hz). To avoid the evaporation of water, mineral oil coated the edge of the cone-plate geometry. Each measurement was repeated three times. Data were processed using Origin™ 8 software.

Thioflavin T (ThT) Spectroscopy Assay: For ThT binding analysis, 10 µl of guar gum-peptide solution (1% w/v) was drop-cast on Greiner bio-one black 96-well flat-bottomed plate. Then, 5 µl of ThT was immediately added to the sample and left stir for 3 min. ThT binding assay was monitored by exciting the sample at 440 nm (5 nm band-pass) and recording the emission fluorescence spectrum from 460 to 600 nm, by using an Infinite M200 PRO plate reader (Tecan). Measurements were performed in triplicate, normalized over ThT-alone fluorescence, and processed with Origin™ 8 software.

FT-IR spectroscopy: The guar gum-peptides were dissolved in distilled water (GIBCO®) to a final concentration of 1% (w/v). All spectra were recorded in attenuated total reflection (ATR) using a PerkinElmer Spectrum 100 spectrometer. A 2 µl aliquot of guar gum-peptide solution was deposited on the reflection diamond element, then allowed to dry. Measurements were performed using a 4 cm^{-1} spectrum resolution, 25 kHz scan speed, 1,000-scan co-addition, triangular apodization, and by averaging 20 scans. All the obtained spectra were reported after ATR correction, smoothing and automatic baseline correction using Origin™ 8 software. Each sample preparation was repeated three times.

CD spectroscopy: The guar gum-peptides were dissolved in distilled water (GIBCO®) to a final concentration of 1% (w/v). CD spectra were collected by a Jasco J-810 (Jasco, Tokyo,

Japan) spectropolarimeter, using quartz cuvettes with an optical path length of 0.1 mm (Hellma Analytics). Data acquisition was performed in continuous scanning mode (190-300 nm) at 25 °C, with a spectral bandwidth of 1 nm and an averaging time of 3 s. The spectrum of each sample was collected three times, averaged, and subtracted from the reference spectrum in distilled water. Data processing was performed using Origin™ 8 software. Estimation of the peptide secondary structure was achieved by using Raussens *et al* method.[52]

Turbidity assay: 200 µl of guar gum, peptide, and different ratios of guar gum-peptide solutions were prepared as described above and put into a 96-well plate. Absorbance at 405 nm was measured every 60 s using an Infinite M200 PRO plate reader (Tecan).

Atomic Force Microscopy (AFM): AFM measurements were performed in tapping mode by using a Multimode Nanoscope V system (Digital Instrument, Veeco), using single-beam silicon cantilever probes (Bruker RFESP-75 0.01-0.025 Ohm-cm Antimony (n) doped Si, cantilever f0, resonance frequency 75 kHz, constant force 3 N m^{-1}). The guar gum-peptide samples were dissolved in distilled water (GIBCO®) a day prior to imaging and incubated at 4 °C. AFM images were taken by depositing 5 µl solutions (final concentration of 0.01% w/v) onto freshly cleaved mica. The samples were kept on the mica for 5 min; subsequently they were rinsed with distilled water to remove loosely bound guar gum-peptides, and then dried under ambient conditions for 30 min. The images were analyzed and visualized using Nanoscope Software and Origin™ 8 software.

Scanning Electron Microscopy (SEM): The guar gum-peptide hydrogel was plunge in liquid nitrogen and then lyophilized. The dried sample was sputter coated with ~8 nm of Au prior to examination using a field-emission SEM (Tescan Vega) operating at 20 kV.

RESULTS AND DISCUSSION

Based on the different molecular structures of GG and SAP alone, we chose to mix the two components at various ratios (e.g. 1:0, 1:0.25, 1:0.5, 1:0.75, 1:1, 1:2, and 1:3). At all tested GG-SAP ratios, the hydrogel composites appeared homogenous. By using turbidity assay, we monitored the time-dependent absorbance of GG-SAP solutions at 405 nm for transparency change. All composite hydrogels were relatively transparent gels; the absorbance remained constant over time with optical density (OD) values ranging from 0.08 to 0.5 (Figure S1). No segregation or phase-separation occurred in any of the composite hydrogels following sonication, suggesting that these constructs form homogeneous well-mixed biomaterials (see Materials and Methods for further details on preparation of GG-SAP composite hydrogels). Looking at their mechanical properties, the viscosity of the various GG-SAP hydrogels was analyzed and compared to that of the pure GG and SAP hydrogels. All hydrogels showed non-Newtonian shear-thinning behavior with a decrease of viscosity as the shear-rate increase (Figure 1a). All composite hydrogels showed increased viscosity levels compared to SAP and GG alone, matched by SAP ratio increments, except for GG-SAP 1:2 and 1:3 (Figure 1b). Indeed, GG-SAP 1:2 and 1:3 showed viscosity values of 0.6 and 0.1 Pa.s, resembling those of SAP hydrogel alone (0.05 Pa.s). This finding is likely ascribable to the prevalence of the SAP mechanical-weak component. Instead, the GG-SAP hydrogel at 1:1 ratio exhibited the highest viscosity values (8.5 Pa.s) at low shear rates, showing a not-sharp decrease with increasing shear rates compared to the other samples, probably due to the "solid-like behavior" of the composite hydrogel. We next measured the mechanical stiffness of the different GG-SAP hydrogels using oscillatory shear rheological experiments. In each composite hydrogel, the trends of elastic (*G'*) and loss (*G"*) moduli showed typical hydrogel profiles, featuring a predominant solid-elastic behavior (*G'*) as

compared to the viscous component (*G"*). Indeed, *G'* values were generally one order of magnitude greater the *G"* (Figure S2). As expected, SAP and GG alone, being soft hydrogels displayed low elastic shear modulus of ~0.2 kPa and ~1 kPa respectively (Figure 1c). On the other hand, the GG-SAP 1:0.25, 1:0.5, and 1:0.75 composites showed a slight increase in the elastic shear modulus throughout tested frequency range (0.1-1,000 Hz) at fixed strain (1%), with *G'* values ranging from 2 to 30 kPa, indicating a synergic effect of GG and SAPs in terms of rheological properties of the GG-SAP scaffolds. Notably, GG-SAP hydrogel at 1:1 ratio showed significantly higher stiffness, with *G'* > 60 kPa (~59-fold higher than GG and SAP alone), probably due to the increased number of interactions between GG and SAP molecules, which contributed to the formation of tougher supramolecular hydrogels. Likely, GG is adsorbed on the long axis of the SAP fibers through H-bonding between carboxylic acid groups of SAP (aspartic acid) with -OH groups along the GG chains (Scheme S1), [32] yielding to an overall reinforcement of mechanical properties of the composite hydrogel.

On the contrary, increasing the peptidic component inside the composite mixture (i.e. 1:2, and 1:3) led to overall decreased mechanical properties (*G′* ~4 kPa) (Figure 1d). This variation of hydrogel stiffness related to the ratio variation between GG ad SAP may be useful for the design of bioprosthetics, 3D cell cultures systems with tuned mechanical properties and beyond.[53]

A similar trend of *G′* reinforcement was obtained also by mixing the plain LDLK12-peptide sequence (with no FAQRVPP functional motif) with GG (Figure S3a-b), demonstrating the validity of this approach for other LDLK12-based SAPs.

Thioflavin-T (ThT) binding assay, enabling the evaluation of the amyloidogenic structures and cross-β fibril formation of materials (see Materials and Methods), was performed to investigate the influence of GG on the self-assembling propensity of SAP into cross-β structures. At all

tested GG-SAP ratios, ThT assay showed typical amyloid-binding emission signal (peak at ~490 nm) testifying the β-rich nature of composite hydrogels resembling the characteristic profile of SAP hydrogel (Figure 2a). No signal has been detected for GG alone, due to its polysaccharide nature. Further, ThT-binding assay was performed to investigate the influence of GG on the plain LDLK12-peptide sequence. Also in this case, ThT assay showed typical amyloid-binding emission signal (peak at ~490 nm) testifying the β-rich nature of composite hydrogels (Figure S3c) and a similar profile to FAQRVPP-LDLK12 hydrogel.

CD spectroscopy in the far UV region of 190-260 nm was also carried out to better analyze the secondary structure of GG-SAP while in solution (see Materials and Methods for details): all GG-SAP composite hydrogels exhibited a CD pattern comprising a negative peak near 218 nm and a positive peak at 195 nm characteristic of β-sheet conformations (Figure 2b). Thus, the CD spectra are in accordance with ThT binding assay. Further, by using Raussens et al method[52] we estimated the percentage of secondary structures from CD spectra; GG-SAP spectra at 1:0, 1:0.25, 1:0.5, 1:0.75, and 1:1 ratio display 74% of β-sheet structures, 12.5% of β-turn structures, and 13.5% of random coil conformation. Whereas GG-SAP spectra at 1:2 and 1:3 ratio display 47% of β-sheet structures, 12.5% of β-turn structures, and 37.9% of random coil conformation.

We then used FT-IR spectroscopy to better characterize the underlying mechanism of GG-SAP self-assembling and to evaluate the incorporation of GG in the SAP fibrils network (Figure 2c). The FT-IR spectrum of SAP alone showed antiparallel β-sheet features with a sharp Amide I band at 1,620 cm^{-1} and a shoulder at 1,695 cm^{-1}. The β-sheet aggregation was also confirmed by the presence of an Amide II band at 1,540 cm^{-1} directly related to CN stretching and NH bending, as we previously reported.[44] The FT-IR spectrum of GG showed a broad absorption band at 1,647 cm^{-1} associated with hydroxyl bending, and three bands at 1,402 (assigned to CH

bending), 1,318, and 1,301 cm^{-1} (C-O-C stretching vibration).[54] Nevertheless, we detected a FT-IR spectra difference between the GG-SAP 1:0.25, 1:0.5, 1:0.75, 1:1 composites and SAP alone (Figure S4a): these four composite hydrogels displayed a sharp Amide I band at 1,647 cm^{-1} and a shoulder at 1,630 cm^{-1}, ascribable to hydroxyl bending and β-sheet features respectively. These changes in the characteristic peptide FT-IR absorption peaks in the Amide I region, could reflect the interaction of GG with carbonyl groups from aspartic acids of SAP molecules. Nonetheless, the predominant β-sheet aggregation of GG-SAP supramolecular hydrogels was still corroborated by the presence of an Amide II band at 1,540 cm^{-1}. Furthermore, the presence of the CH bending and C-O-C stretching bands at 1,402, 1,318, and 1,301 cm^{-1}, which are not present in the SAP spectrum, confirmed incorporation of GG in the SAP fibrils network (Figure S4b). Contrarily, GG-SAP 1:2 and 1:3 composites exhibited FT-IR absorption peaks at 1,620 cm^{-1} (Amide I), 1,540 cm^{-1} (Amide II), and a lowering of the CH bending and C-O-C stretching signals ascribable to GG (Figure S4a-b), highlighting a predominance of the SAP structural patterns, as also suggested by rheological data. Hence, ThT-binding assay, CD, and FT-IR analysis confirmed β-sheet self-aggregation of SAP in all tested GG-SAPs, suggesting that the introduction of GG did not affect the macromolecular organization of the supramolecular composite hydrogels.

We further examined the thermal responsive gel-sol transitions of GG-SAP composites (Figure 3). The pure GG and SAP hydrogels underwent gel-sol transitions during cycles of heating-cooling process (see Materials and Methods). The consistent loss of the viscous-elastic properties of SAP hydrogel above 45 °C displayed a drastic decrease of the gel state and an irreversible gel-sol transition (Figure 3a). This is likely because LDLK-based SAPs are highly hydrated hydrogels, containing up to 99.5% (w/v) water, with modest self-healing propensity since

nanostructures from short linear LDLK12-based SAPs are led by weak transient non-covalent interactions and, as such, can undergo irreversible structural changes (e.g. from β-sheet to random coil structure) when subjected to temperatures above 50 °C. Instead, the gel state of high-molecular weight GG became viscous-liquid when heated over 60 °C, and reformed after cooling below 25 °C, thus preserving its mechanical behavior (Figure 3b). This thermal responsive capability, repeated over times, is due to reversible and exothermic reactions between hydroxyl groups of GG and $B(OH)_4$ of borax.[55] Interestingly, GG-SAP composites at 1:0.25, 1:0.5, and 1:0.75 ratios maintained the thermal responsiveness of GG (Figure S5a), but an important difference: the GG-SAP hydrogel at 1:1 ratio showed a reversible rapid transformation of gel state into solvent, followed by a still reversible reformation of a gel state at temperatures above 60 °C (Figure 3c). This dynamically reversible trend may be due to the initial loss of water from the peptide, leading to an overall shrinkage of the sample, probably causing an increase in the density of supramolecular interactions between $B(OH)_4$ and hydroxyl and/or carbonyl groups of respectively borax and GG-SAP. On the other hand, the GG-SAP composites at 1:2 and 1:3 ratio lack any full gel recovery after heating and cooling (Figure S5b), further confirming, as suggested by rheological and FT-IR results, their chemical-physical similarities with standard SAPs.

In addition to thermal responsive performance, GG-SAP composite hydrogels also exhibited a remarkable self-healing propensity. The self-healing capacity of GG-SAP supramolecular hydrogels was investigated by standard empirical tests and rheological measurements (see Materials and Methods). The elastic response of GG-SAP composites was studied through continuous step strain measurements (Figure 4a). Initially, the GG-SAPs were deformed under small amplitude oscillatory deformation (ω= 1 Hz, γ = 10%, 300 s), showing solid nature with *G'*

of 60 kPa. When exerting larger amplitude oscillatory deformation (ω = 1 Hz, γ = 100%, 300 s) the *G'* value decreased to about 0.3 kPa, implying that the hydrogel lost parts of its mechanical stability (as shown in strain sweep test; Figure S6a). After decreasing the amplitude oscillatory deformation (ω = 1 Hz, γ = 10%, 300 s), *G'* returned to its original values immediately, demonstrating a rapid recovery of the mechanical properties of GG-SAP given by its internal network capable of forming dynamic covalent bonds. The above process could be repeated multiple time (>20) without any appreciable fatigue-related phenomenon (Figure S6b). On the contrary, SAP hydrogel showed no recovery property when subjected to continuous step strain cycles: *G'* modulus did not recover to its original values with fast kinetics seen with GG-SAP, because of the weak and brittle nature of SAPs. In order to better demonstrate the excellent self-healing ability of GG-SAP, two GG-SAP hydrogels (with and without methylene blue dying) were cut into two pieces, and two halves from different hydrogels were brought into contact (Figure 4b, and Figure S6c). After 5 min, damaged pieces adhered and healed to one integral hydrogel without using any external force or stimulus. To test the integrity property of the healed hydrogel, it was subjected throughout a 0.1-1,000 Hz frequency range at fixed strain (1%). The G' of healed GG-SAP remained close to the values of native hydrogel before rupture (Figure S6d). More remarkably, this self-healed hydrogel could withstand bending, stretching and was capable of supporting its own weight against gravity without further interior or exterior cracks (Figure 4c): this implied that 3D network structures, as well as mechanical strength of the hydrogels, were optimally recovered.

Due to the dynamic properties of GG-SAP hydrogels, we also looked at the stress-relaxation profile, being considered as crucial property for cell ingrowth and migration within implanted scaffolds in tissue engineering applications.[44] Each sample was deformed at 1 mm min^{-1} rate

up to 5 %, 10 % and 100 % strain, held constant for 120 s, while stress-relaxation curve was measured (Figure 4d). For each strain condition it takes about 30-40 s for the stress relaxation process to be completed. As expected, SAP alone showed stress relaxation propensity at 5% strain only. This tunability of stress-relaxation profiles for GG-SAP composites could be relevant for 3D printing, since a pressure-holding stage during embossing is generally required, or for 3D cell behavior studies, since cells usually respond to oscillation forces in a few seconds, exert traction forces on timescales of minutes, and undergo proliferation/spreading on minutes-to-hours timescales.

Structural morphologies of the composite hydrogels were investigated via AFM and SEM, allowing to examine size and height distribution of the GG-SAP assemblies (Figure 5). All composite hydrogels showed well-defined entangled nanofibrous structures with ~8 nm in average width distributions (Figure 5a) and ~0.4-2.1 nm in height (Figure 5b), similar to previously reported values of SAP fibrils.[44] Also, morphological analysis of GG mixed with the plain LDLK12-peptide showed well-defined entangled nanofibrous structures as well (Figure S3d-e-f). In addition, morphologies of GG-SAP at 1:1 ratio, as observed by SEM images (Figure S7), were in good agreement with the results of the AFM analysis, with 0.8 nm average height. Overall, these morphological analyses confirmed the assembly propensity of all GG-SAP hydrogels, suggesting that GG did not hamper the formation of clustered nanofibers.

Thanks to the physicochemical reinforcement of rationally designed FAQRVPP-LDLK12 peptide (and of the plain LDLK12) with guar gum, it was possible to nano-fabricate diverse free-shapeable, self-standing, self-adhesive, and flexible GG-SAP constructs (Figure 6). In our opinion, these supramolecular hydrogels could be a valuable option for wound healing aiming to primarily maintain the moisture at wound sites (thanks to their high water content - 99.5%),

manage exudates, and to exert contractile forces sufficient to promote active wound closure, since they are mechanically robust, tough, and strongly adhesive. Further, as these supramolecular composite hydrogels can respond to physiological signs, including strains and temperature, they could be used as touch and strain sensors, or as a gel-like, aquatic, stretchable and self-healing electronic skin.[56] Lastly, though the GG alone has been successfully studied as a matrix for colon-specific treatment, the improvement of biomechanical and shear-thinning behaviors reported here make this composite GG-SAP scaffold prone to be used as gel cushion to reduce the risk of tearing the colon during endoscopy procedures for removing polyps.[57, 58]

CONCLUSIONS

In summary, this study aimed at designing new composite hydrogels by combining the favorable multi-stimuli responsive properties of the natural GG and the assets of FAQRVPP-LDLK12 SAP. The feasible formation of such supramolecular composite biomaterials was demonstrated by rheological measurements, CD spectroscopy, FT-IR spectroscopy, AFM, and SEM analysis. GG improves the recovery of the composite hydrogel after shear, its thermo-responsive capability, and its mechanical strength and processability, whereas SAP improves the composite hydrogel's shear thinning behavior, and contributes to the formation of well-defined entangled nanofibrous structures.

Being our findings valid for the LDLK12-alone SAPs too, the present work not only exemplifies a feasible strategy to explore the effect of naturally occurring polysaccharides - as Guar Gum - on SAPs, but also may lay the basis for various future applications of supramolecular composite polysaccharide-peptide hydrogels including biochips, substrates for culturing synthetic meat, biosensors, and for drug delivery.

ASSOCIATED CONTENT

Supporting Information.

The following files are available free of charge: turbidity assay, rheological characterization, FT-IR absorption peaks, thermal-responsive performance, dynamic strain amplitude cyclic test, and SEM analysis.

Author Contributions

R.P. conceived the project and performed the experiments. R.P. and F.G. designed the experiments, evaluated the data, and wrote the manuscript. F.G. supervised the project.

Funding Sources

The work described and performed by R.P., and F.G. was funded by the "Ricerca Corrente" funding granted by the Italian Ministry of Health and by the "5 × 1000" voluntary contributions. Financial support also came from Revert onlus.

ACKNOWLEDGMENT

We are grateful to Prof. Luca Beverina for allowing our FT-IR experiments to be performed at his facility at the Material Science Department of the University of Milan-Bicocca, and to Dr. Carmen Lammi and Prof. Anna Arnoldi for allowing our CD experiments at Department of Pharmaceutical Sciences, University of Milan.

ORCID

R.Pugliese https://orcid.org/0000-0001-7669-4457 ;

F.Gelain https://orcid.org/0000-0002-2624-5853 ;

GRAPHICAL ABSTRACT

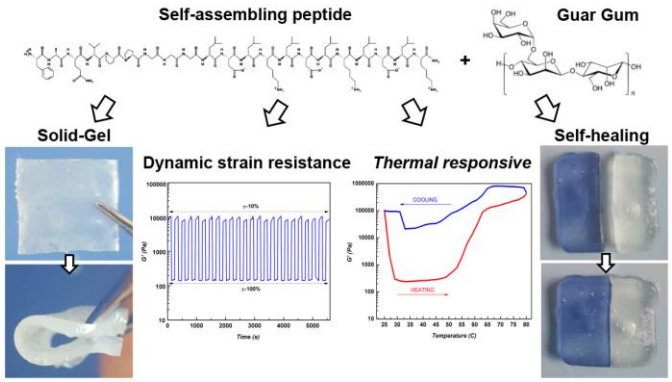

FIGURES

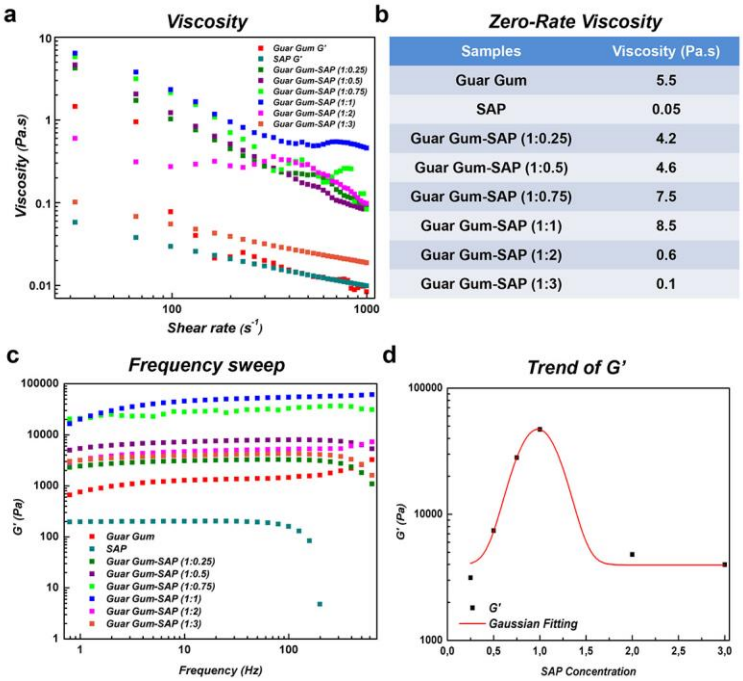

Samples	Viscosity (Pa.s)
Guar Gum	5.5
SAP	0.05
Guar Gum-SAP (1:0.25)	4.2
Guar Gum-SAP (1:0.5)	4.6
Guar Gum-SAP (1:0.75)	7.5
Guar Gum-SAP (1:1)	8.5
Guar Gum-SAP (1:2)	0.6
Guar Gum-SAP (1:3)	0.1

Figure 1. Mechanical properties of GG-SAP composite hydrogels. (a) Viscosity measurements at increasing shear rate of GG, SAP, and 1:0.25, 1:0.5, 1:0.75, 1:1, 1:2, and 1:3 composites. (b) Calculation of zero-rate viscosity. (c) Frequency sweep experiments of hydrogels recorded as a function of angular frequency (0.1-1,000 Hz) at fixed strain of 1%. (d) Trend of elastic (*G'*) modulus of composite supramolecular hydrogels.

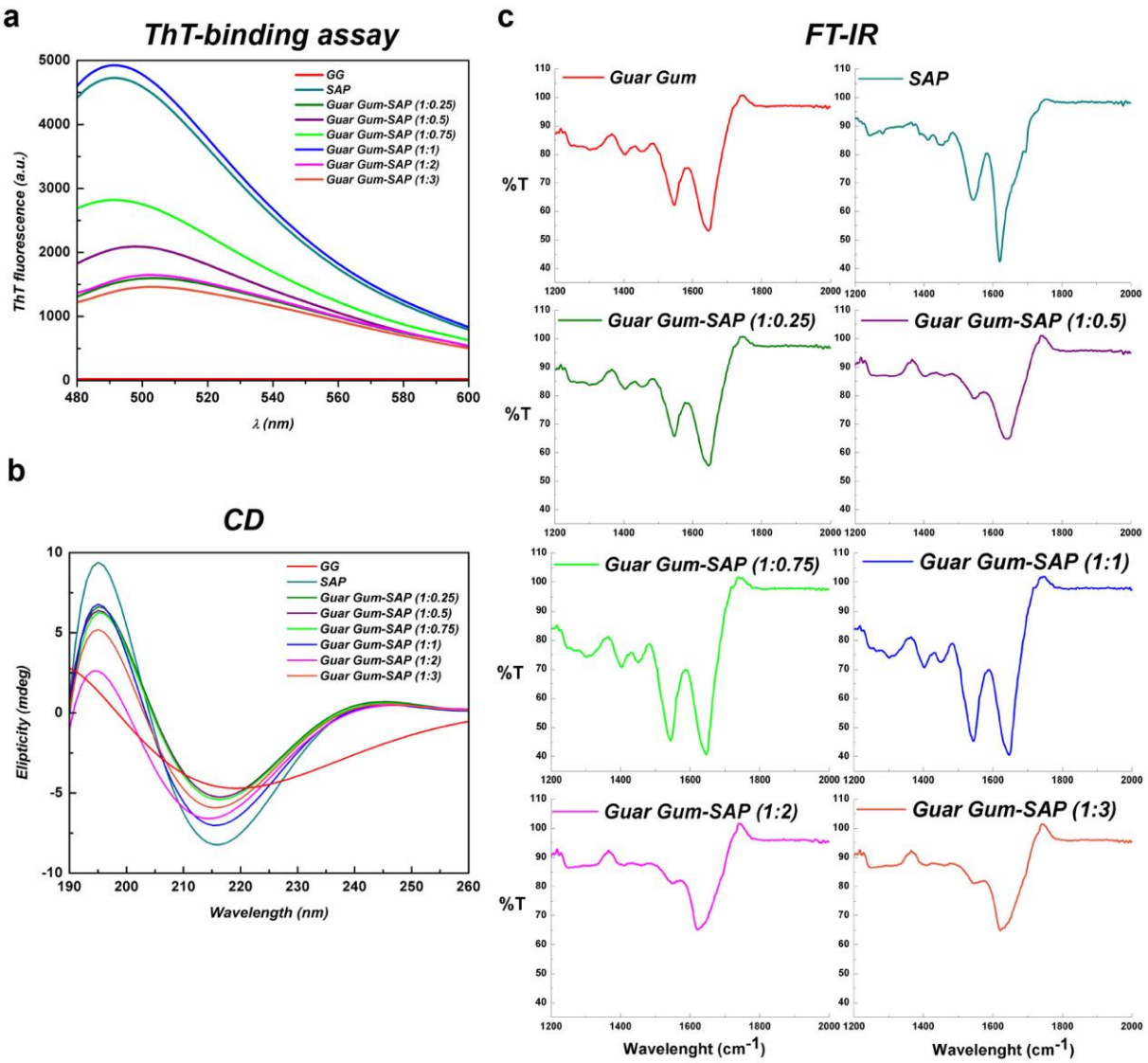

Figure 2. Supramolecular organization of GG-SAP composite hydrogels. (a) ThT emission spectra of supramolecular GG-SAP composite hydrogels; all tested GG-SAP ratios show amyloid-binding emission signal establishing the β-rich nature of composite hydrogels. (b) CD and (c) FT-IR spectra of the GG-SAP composites in solution, showing the presence of β-sheet assemblies.

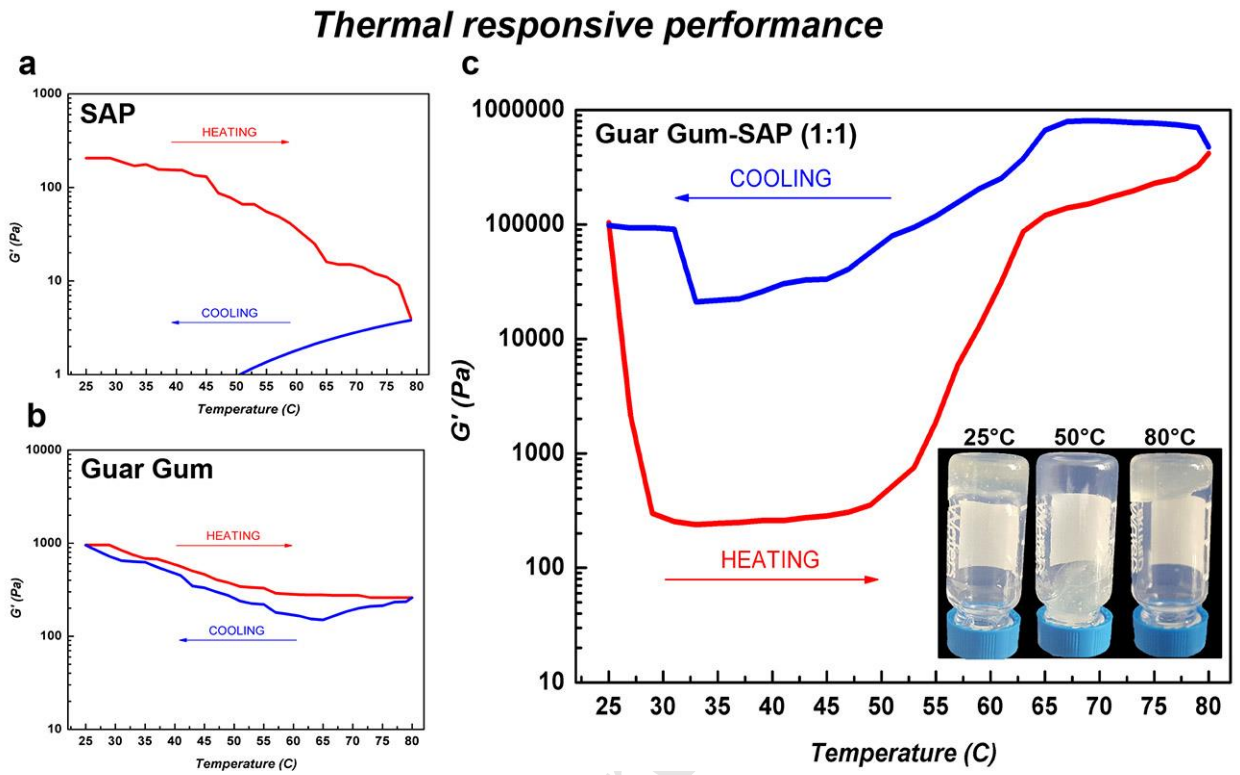

Figure 3. Thermal-responsive performance of GG-SAP composite hydrogels. (a) Cycles of heating-cooling process of SAP hydrogel showing its irreversible gel-sol transition concurrently with a consistent loss of viscous-elastic properties. Gel-sol transitions capability of (b) GG and (c) GG-SAP (1:1) composite during cycles of heating-cooling process with preserved mechanical behavior.

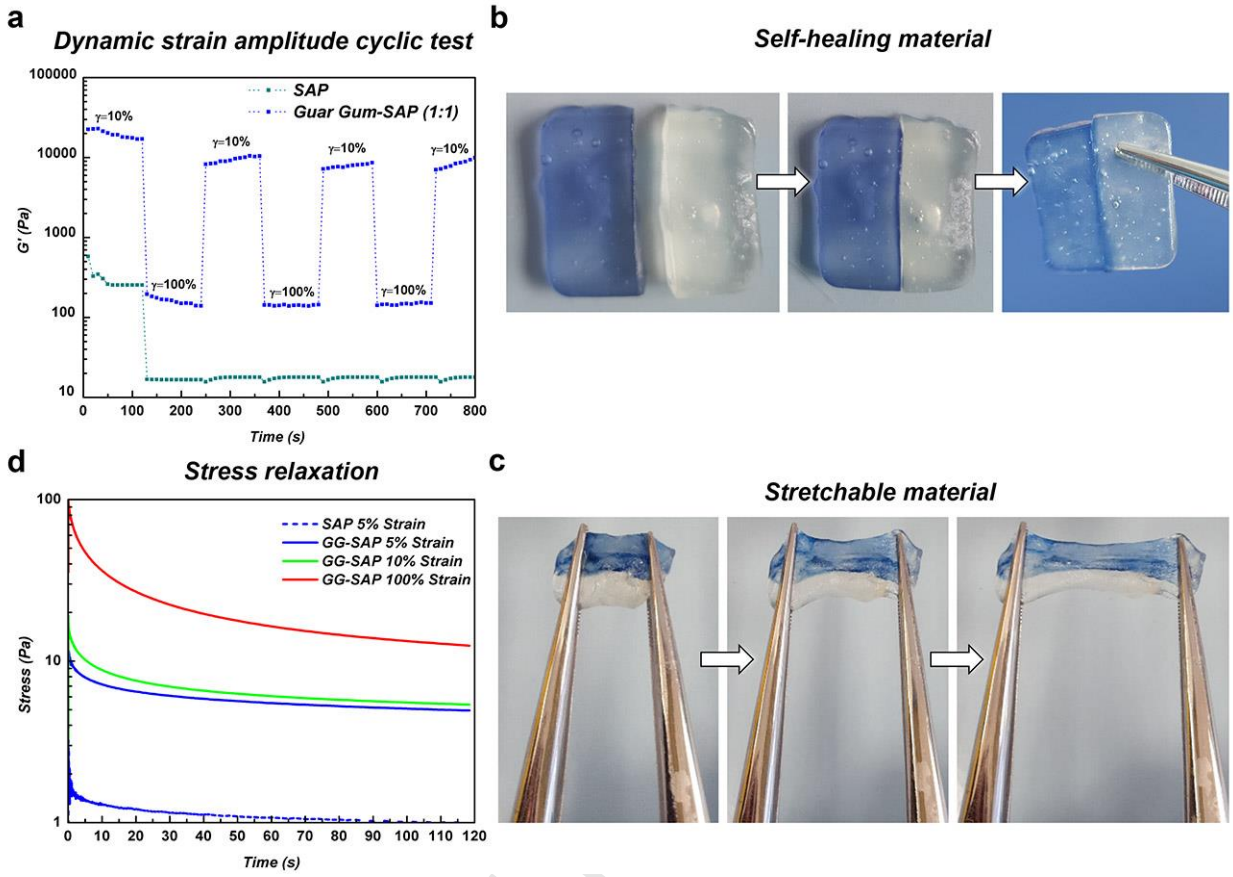

Figure 4. Self-healing behavior of GG-SAP composite hydrogels. (a) Self-healing property of SAP alone, and GG-SAP (1:1) composite hydrogel verified via continuous step strain measurements (ω= 1Hz, γ=10%, 300 s, and ω=1Hz, γ=100%, 300 s). (b) Autonomous healing of native GG-SAP hydrogels (with and without dying by methylene blue), at room temperature for 5 min without using any external force or stimulus. (c) Stretchable property of self-healing GG-SAP composite hydrogels. (d) Stress relaxation curves of SAP alone, and GG-SAP hydrogel (1:1) deformed 1 mm min^{-1} at 5%, 10% and 100% strain held constant for 120 s.

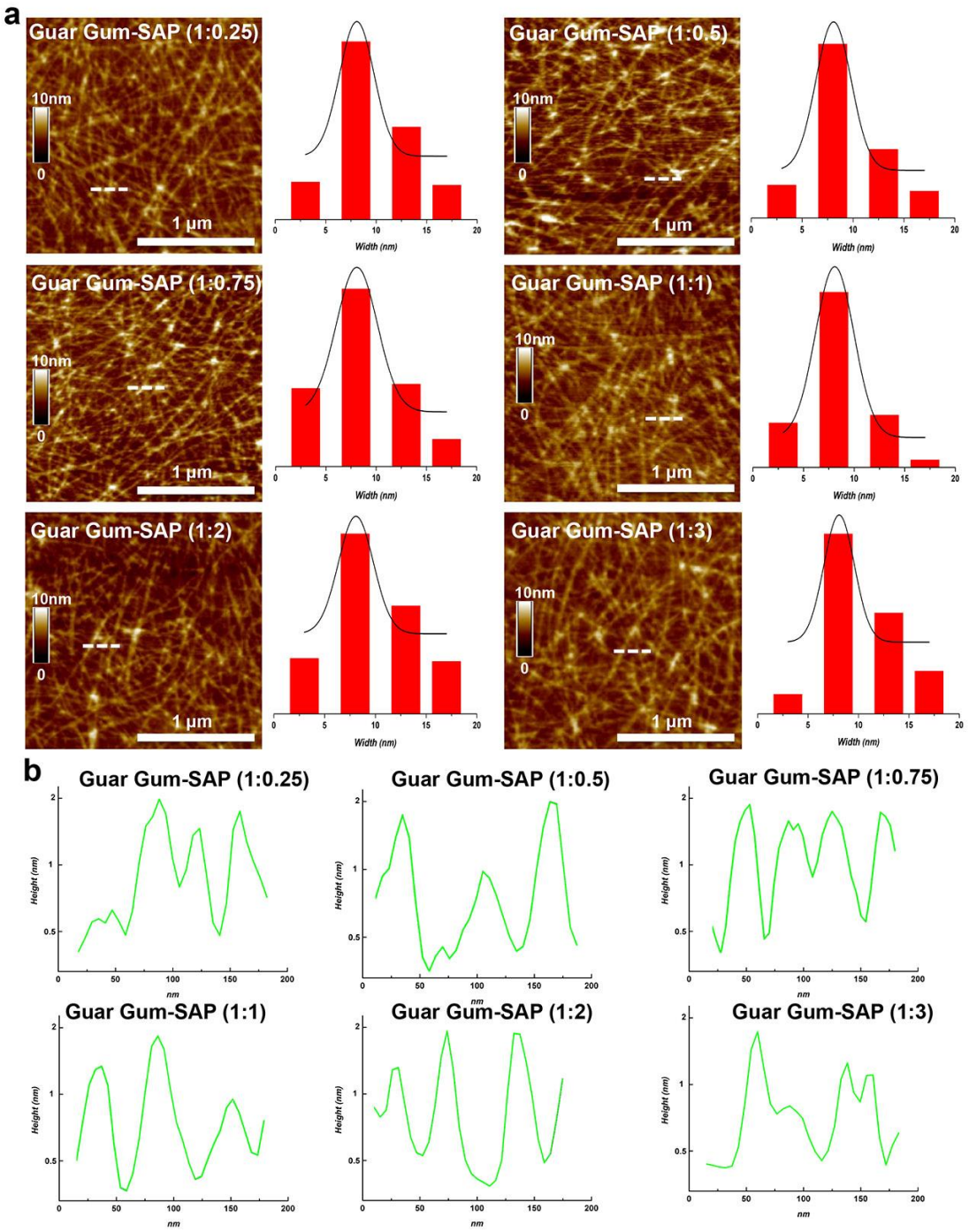

Figure 5. Atomic Force Microscopy analysis of GG-SAP composite hydrogels. (a) AFM images and width distribution of GG-SAP 1:0.25, 1:0.5, 1:0.75, 1:1, 1:2, and 1:3 composites. (b) Height measurements of GG-SAP composite hydrogels.

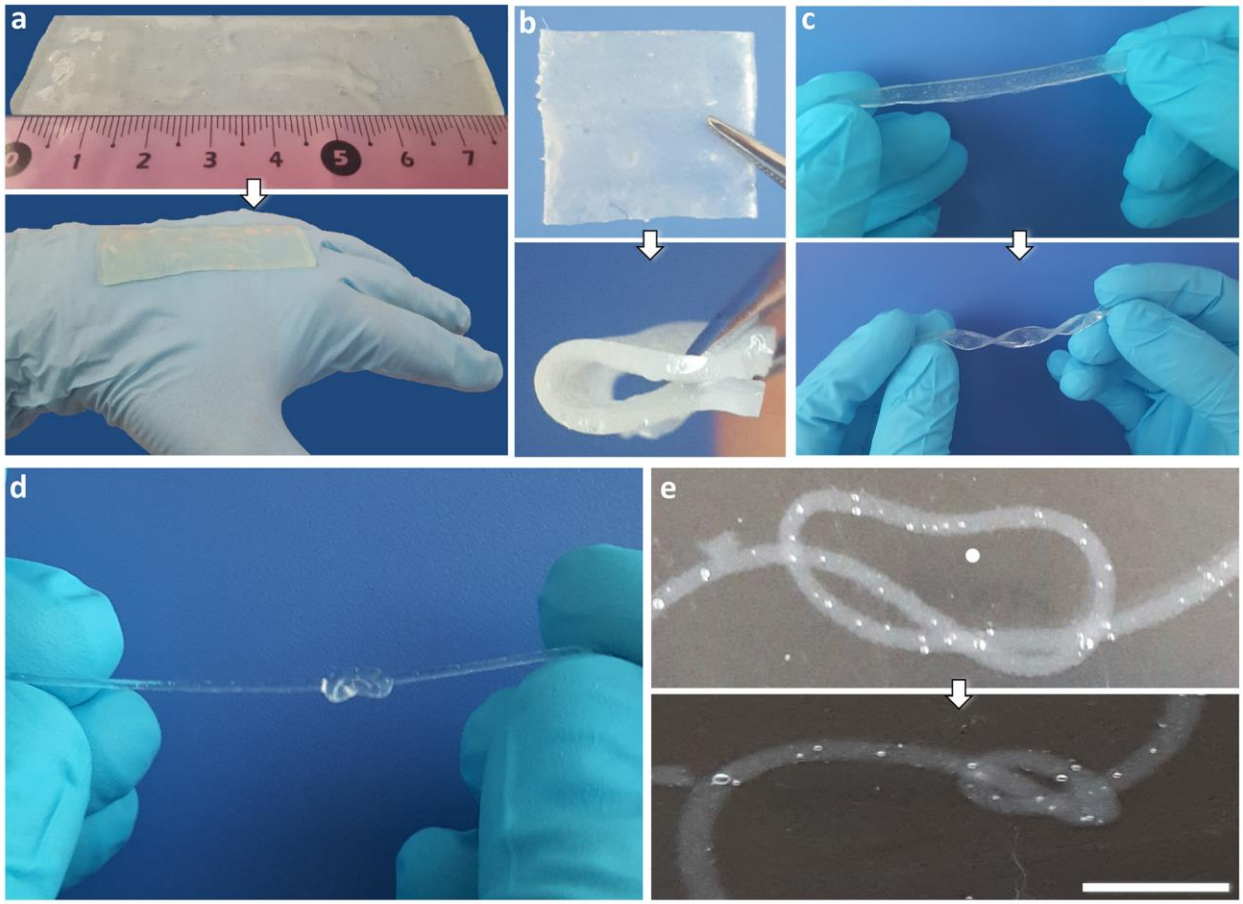

Figure 6. Fabrication of free-shapeable and self-sustaining GG-SAP composite hydrogels showing potential use as (a) Self-adhesive gel-like bandage. (b) Flexible gel-like patch. (c) Twisted gel-like scaffold. (d) Gel-like wire. (e) High magnification of nanostructured wire knot formation (1 cm scale bar).

REFERENCES

[1] Webber MJ, Appel EA, Meijer EW, Langer R. Supramolecular biomaterials. Nature materials. 2016;15:13-26.

[2] Webber MJ, Dankers PYW. Supramolecular Hydrogels for Biomedical Applications. Macromolecular bioscience. 2019;19:e1800452.

[3] Shi Y, Wang Z, Zhang X, Xu T, Ji S, Ding D, et al. Multi-responsive supramolecular hydrogels for drug delivery. Chemical communications. 2015;51:15265-7.

[4] Basak S, Nandi N, Paul S, Hamley IW, Banerjee A. A tripeptide-based self-shrinking hydrogel for waste-water treatment: removal of toxic organic dyes and lead (Pb(2+)) ions. Chemical communications. 2017;53:5910-3.

[5] Yuk H, Lu B, Zhao X. Hydrogel bioelectronics. Chemical Society reviews. 2019;48:1642-67.

[6] Lehn JM. Supramolecular Chemistry—Scope and Perspectives Molecules, Supermolecules, and Molecular Devices (Nobel Lecture). Angewandte Chemie. 1988;27:89-112.

[7] Aida T, Meijer EW, Stupp SI. Functional supramolecular polymers. Science. 2012;335:813-7.

[8] Zhang S. Discovery and design of self-assembling peptides. Interface focus. 2017;7:20170028.

[9] Pugliese R, Gelain F. Peptidic Biomaterials: From Self-Assembling to Regenerative Medicine. Trends in biotechnology. 2017;35:145-58.

[10] Zhang S. Fabrication of novel biomaterials through molecular self-assembly. Nat Biotechnol. 2003;21:1171-8.

[11] Zhang S, Holmes T, Lockshin C, Rich A. Spontaneous assembly of a self-complementary oligopeptide to form a stable macroscopic membrane. Proceedings of the National Academy of Sciences of the United States of America. 1993;90:3334-8.

[12] Zhang S, Holmes TC, DiPersio CM, Hynes RO, Su X, Rich A. Self-complementary oligopeptide matrices support mammalian cell attachment. Biomaterials. 1995;16:1385-93.

[13] Gelain F, Horii A, Zhang S. Designer self-assembling peptide scaffolds for 3-d tissue cell cultures and regenerative medicine. Macromolecular bioscience. 2007;7:544-51.

[14] Kisiday J, Jin M, Kurz B, Hung H, Semino C, Zhang S, et al. Self-assembling peptide hydrogel fosters chondrocyte extracellular matrix production and cell division: implications for cartilage tissue repair. Proceedings of the National Academy of Sciences of the United States of America. 2002;99:9996-10001.

[15] Lammi C, Bollati C, Gelain F, Arnoldi A, Pugliese R. Enhancement of the Stability and Anti-DPPIV Activity of Hempseed Hydrolysates Through Self-Assembling Peptide-Based Hydrogels. Frontiers in chemistry. 2018;6:670.

[16] Wang R, Wang Z, Guo Y, Li H, Chen Z. Design of a RADA16-based self-assembling peptide nanofiber scaffold for biomedical applications. Journal of biomaterials science Polymer edition. 2019;30:713-36.

[17] Hainline KM, Gu F, Handley JF, Tian YF, Wu Y, de Wet L, et al. Self-Assembling Peptide Gels for 3D Prostate Cancer Spheroid Culture. Macromolecular bioscience. 2019;19:e1800249.

[18] Huang LC, Wang HC, Chen LH, Ho CY, Hsieh PH, Huang MY, et al. Bioinspired Self-assembling Peptide Hydrogel with Proteoglycan-assisted Growth Factor Delivery for Therapeutic Angiogenesis. Theranostics. 2019;9:7072-87.

[19] Pugliese R, Bollati C, Gelain F, Arnoldi A, Lammi C. A Supramolecular Approach to Develop New Soybean and Lupin Peptide Nanogels with Enhanced Dipeptidyl Peptidase IV (DPP-IV) Inhibitory Activity. Journal of agricultural and food chemistry. 2019;67:3615-23.

[20] Shi Y, Ferreira DS, Banerjee J, Pickford AR, Azevedo HS. Tuning the matrix metalloproteinase-1 degradability of peptide amphiphile nanofibers through supramolecular engineering. Biomaterials science. 2019.

[21] Mansukhani NA, Peters EB, So MM, Albaghdadi MS, Wang Z, Karver MR, et al. Peptide Amphiphile Supramolecular Nanostructures as a Targeted Therapy for Atherosclerosis. Macromolecular bioscience. 2019;19:e1900066.

[22] Zhou S, Hokugo A, McClendon M, Zhang Z, Bakshi R, Wang L, et al. Bioactive peptide amphiphile nanofiber gels enhance burn wound healing. Burns : journal of the International Society for Burn Injuries. 2019;45:1112-21.

[23] Hernandez-Garcia A, Alvarez Z, Simkin D, Madhan A, Pariset E, Tantakitti F, et al. Peptide-siRNA Supramolecular Particles for Neural Cell Transfection. Adv Sci (Weinh). 2019;6:1801458.

[24] So MM, Mansukhani NA, Peters EB, Albaghdadi MS, Wang Z, Perez CMR, et al. Peptide Amphiphile Nanostructures for Targeting of Atherosclerotic Plaque and Drug Delivery. Advanced biosystems. 2018;2.

[25] Hendricks MP, Sato K, Palmer LC, Stupp SI. Supramolecular Assembly of Peptide Amphiphiles. Accounts of chemical research. 2017;50:2440-8.

[26] Moore AN, Hartgerink JD. Self-Assembling Multidomain Peptide Nanofibers for Delivery of Bioactive Molecules and Tissue Regeneration. Accounts of chemical research. 2017;50:714-22.

[27] Okesola BO, Wu Y, Derkus B, Gani S, Wu D, Knani D, et al. Supramolecular Self-Assembly To Control Structural and Biological Properties of Multicomponent Hydrogels. Chemistry of materials : a publication of the American Chemical Society. 2019;31:7883-97.

[28] Lopez-Silva TL, Leach DG, Li IC, Wang X, Hartgerink JD. Self-Assembling Multidomain Peptides: Design and Characterization of Neutral Peptide-Based Materials with pH and Ionic Strength Independent Self-Assembly. ACS biomaterials science & engineering. 2019;5:977-85.

[29] Leach DG, Young S, Hartgerink JD. Advances in immunotherapy delivery from implantable and injectable biomaterials. Acta biomaterialia. 2019;88:15-31.
[30] Adler-Abramovich L, Gazit E. The physical properties of supramolecular peptide assemblies: from building block association to technological applications. Chemical Society reviews. 2014;43:6881-93.
[31] Guterman T, Levin M, Kolusheva S, Levy D, Noor N, Roichman Y, et al. Real-Time In-Situ Monitoring of a Tunable Pentapeptide Gel-Crystal Transition. Angew Chem Int Ed Engl. 2019;58:15869-75.
[32] Chakraborty P, Ghosh M, Schnaider L, Adadi N, Ji W, Bychenko D, et al. Composite of Peptide-Supramolecular Polymer and Covalent Polymer Comprises a New Multifunctional, Bio-Inspired Soft Material. Macromolecular rapid communications. 2019;40:e1900175.
[33] Basavalingappa V, Guterman T, Tang Y, Nir S, Lei J, Chakraborty P, et al. Expanding the Functional Scope of the Fmoc-Diphenylalanine Hydrogelator by Introducing a Rigidifying and Chemically Active Urea Backbone Modification. Adv Sci (Weinh). 2019;6:1900218.
[34] Hsu BB, Conway W, Tschabrunn CM, Mehta M, Perez-Cuevas MB, Zhang S, et al. Clotting Mimicry from Robust Hemostatic Bandages Based on Self-Assembling Peptides. ACS nano. 2015;9:9394-406.
[35] Yang S, Wei S, Mao Y, Zheng H, Feng J, Cui J, et al. Novel hemostatic biomolecules based on elastin-like polypeptides and the self-assembling peptide RADA-16. BMC biotechnology. 2018;18:12.
[36] Walvekar P, Gannimani R, Rambharose S, Mocktar C, Govender T. Fatty acid conjugated pyridinium cationic amphiphiles as antibacterial agents and self-assembling nano carriers. Chemistry and physics of lipids. 2018;214:1-10.
[37] Jiang T, Shen S, Wang T, Li M, He B, Mo R. A Substrate-Selective Enzyme-Catalysis Assembly Strategy for Oligopeptide Hydrogel-Assisted Combinatorial Protein Delivery. Nano letters. 2017;17:7447-54.
[38] Ozeki M, Kuroda S, Kon K, Kasugai S. Differentiation of bone marrow stromal cells into osteoblasts in a self-assembling peptide hydrogel: in vitro and in vivo studies. J Biomater Appl. 2011;25:663-84.
[39] Ellis-Behnke RG, Liang YX, Tay DK, Kau PW, Schneider GE, Zhang S, et al. Nano hemostat solution: immediate hemostasis at the nanoscale. Nanomedicine. 2006;2:207-15.
[40] Schneider A, Garlick JA, Egles C. Self-assembling peptide nanofiber scaffolds accelerate wound healing. PloS one. 2008;3:e1410.
[41] Ichihara Y, Kaneko M, Yamahara K, Koulouroudias M, Sato N, Uppal R, et al. Self-assembling peptide hydrogel enables instant epicardial coating of the heart with mesenchymal stromal cells for the treatment of heart failure. Biomaterials. 2018;154:12-23.
[42] Li XC, Wu YH, Bai XD, Ji W, Guo ZM, Wang CF, et al. BMP7-Based Functionalized Self-Assembling Peptides Protect Nucleus Pulposus-Derived Stem Cells From Apoptosis In Vitro. Tissue engineering Part A. 2016;22:1218-28.
[43] Pugliese R, Marchini A, Saracino GAA, Zuckermann RN, Gelain F. Cross-linked self-assembling peptide scaffolds. Nano Research. 2018;11:586–602.
[44] Pugliese R, Maleki M, Zuckermann RN, Gelain F. Self-assembling peptides cross-linked with genipin: resilient hydrogels and self-standing electrospun scaffolds for tissue engineering applications. Biomaterials science. 2018;7:76-91.
[45] Thombare N, Jha U, Mishra S, Siddiqui MZ. Guar gum as a promising starting material for diverse applications: A review. International journal of biological macromolecules. 2016;88:361-72.
[46] Murali R, Vidhya P, Thanikaivelan P. Thermoresponsive magnetic nanoparticle--aminated guar gum hydrogel system for sustained release of doxorubicin hydrochloride. Carbohydrate polymers. 2014;110:440-5.
[47] Das S, Subuddhi U. pH-Responsive guar gum hydrogels for controlled delivery of dexamethasone to the intestine. International journal of biological macromolecules. 2015;79:856-63.
[48] Krishnaiah YS, Bhaskar Reddy PR, Satyanarayana V, Karthikeyan RS. Studies on the development of oral colon targeted drug delivery systems for metronidazole in the treatment of amoebiasis. International journal of pharmaceutics. 2002;236:43-55.
[49] Krishnaiah YS, Veer Raju P, Dinesh Kumar B, Satyanarayana V, Karthikeyan RS, Bhaskar P. Pharmacokinetic evaluation of guar gum-based colon-targeted drug delivery systems of mebendazole in healthy volunteers. Journal of controlled release : official journal of the Controlled Release Society. 2003;88:95-103.
[50] Ji C, Xu H, Wu W. In vitro evaluation and pharmacokinetics in dogs of guar gum and Eudragit FS30D-coated colon-targeted pellets of indomethacin. Journal of drug targeting. 2007;15:123-31.
[51] Gelain F, Cigognini D, Caprini A, Silva D, Colleoni B, Donega M, et al. New bioactive motifs and their use in functionalized self-assembling peptides for NSC differentiation and neural tissue engineering. Nanoscale. 2012;4:2946-57.
[52] Raussens V, Ruysschaert JM, Goormaghtigh E. Protein concentration is not an absolute prerequisite for the determination of secondary structure from circular dichroism spectra: a new scaling method. Analytical biochemistry. 2003;319:114-21.
[53] Vining KH, Mooney DJ. Mechanical forces direct stem cell behaviour in development and regeneration. Nature reviews Molecular cell biology. 2017;18:728-42.
[54] LeiDai, Zhang L, BoYang BW, Khan I, Khan A, YonghaoNi. Multifunctional self-assembling hydrogel from guar gum. Chemical Engineering Journal. 2017;330:1044-51.
[55] Dai L, Nadeau B, An X, Cheng D, Long Z, Ni Y. Silver nanoparticles-containing dual-function hydrogels based on a guar gum-sodium borohydride system. Scientific reports. 2016;6:36497.

[56] Yue Cao, Yu Jun Tan, Si Li, Wang Wei Lee, Hongchen Guo, Yongqing Cai, et al. Self-healing electronic skins for aquatic environments. Nature Electronics. 2019;2.
[57] Hattori H, Tsujimoto H, Hase K, Ishihara M. Characterization of a water-soluble chitosan derivative and its potential for submucosal injection in endoscopic techniques. Carbohydrate polymers. 2017;175:592-600.
[58] Pang Y, Liu J, Moussa ZL, Collins JE, McDonnell S, Hayward AM, et al. Endoscopically Injectable Shear-Thinning Hydrogels Facilitating Polyp Removal. Advanced Science. 2019.

Declaration of interests

☒ The authors declare that they have no known competing financial interests or personal relationships that could have appeared to influence the work reported in this paper.

☐The authors declare the following financial interests/personal relationships which may be considered as potential competing interests:

Credit Author Statement

R.P. conceived the project and performed the experiments. R.P. and F.G. designed the experiments, evaluated the data, and wrote the manuscript. F.G. supervised the project.